*Aust. J. Phys.*, 1989, **42**, 73–100

# Experimental Studies of Plasma Confined in a Toroidal Heliac

*B. D. Blackwell, S. M. Hamberger, L. E. Sharp and X.-H. Shi*

Plasma Research Laboratory, Research School of Physical Sciences,
Australian National University, Canberra, A.C.T. 2601, Australia.

*Abstract*

The design, construction and operation of the prototype heliac SHEILA are described. Gas breakdown conditions are compared with high frequency discharges. Plasma isobars obtained from local measurements are shown to agree closely with computed magnetic flux surfaces for a range of magnetic configurations. The effect of changing the configuration on fluctuation mode numbers is demonstrated and shown to be consistent with the calculated rotational transforms.

## 1. Introduction

In recent years plasma physicists have shown renewed interest in toroidal magnetic plasma confinement systems which do not rely on large plasma currents to provide the necessary closed magnetic flux surfaces. Those which involve large plasma currents, such as tokamaks and other pinch devices, are subject to certain forms of gross instability, such as disruptions, which could have potentially serious consequences in reactor application, while the generation of these currents also poses obvious problems to the perceived need for continuous operation.

Those devices which do not involve large plasma currents, generically classed as *stellarators*, produce their closed configuration entirely by the magnetic field due to currents in conductors external to the plasma: this consists essentially of a dominant toroidally directed field combined with significant helical components. The poloidal harmonic contributions ($l$) of this helical field determine the main parameters of the configuration (Carreras *et al.* 1988): in particular, the rotational transform $\iota$ is determined mainly by the lower harmonics. Since a high transform configuration resists the geometric distortion and displacement of the flux surfaces by plasma kinetic pressure, recent emphasis has been on utilising the strong $l = 1$ helical component associated with a helical magnetic axis. Although such systems have been known and studied for many years [indeed Spitzer's (1958) original 'Figure-8' stellarator belongs to this class], for reasons of stability it is necessary to introduce other features, such as a magnetic well and/or shear, into the surfaces.

The heliac coil arrangement (Boozer *et al.* 1983) provides such a configuration. It consists essentially of a set of toroidal field (TF) coils whose centres follow

0004-9506/89/010073$03.00

a helical path about a toroidally directed central conductor or ring core. With appropriate currents in each this leads to a set of toroidal flux surfaces whose axis follows the toroidal field coils and makes a large helical excursion. The cross sections of the flux surfaces, which define the plasma boundary and pressure profile, are deeply indented or 'bean-shaped': such a shape generally results in the formation of significant mean magnetic wells which theory predicts are necessary to stabilize certain fast growing resistive instabilities which are not affected by magnetic shear.

Once the geometry of such a heliac system has been defined there is only a very limited range of magnetic configurations accessible by varying the conductor currents. However, the addition of a further winding to control the $l = 1$ helical field component, such as a single helical conductor around the ring core (Harris *et al.* 1985), enables the important parameters, such as rotational transform, shear, and magnetic well, to be varied over a considerable range. The concept of stabilisation by a mean magnetic well was first discussed in 1964 (Furth and Rosenbluth 1964; Furth *et al.* 1966; McNamara *et al.* 1966), and the basic heliac scheme proposed in Princeton to exploit this emerged some twenty years later (Boozer *et al.* 1983; Yoshikawa 1983), followed by some preliminary design and computational studies (Ehrhardt 1984). However, the first opportunity to test the concept experimentally followed the construction in 1984 of the apparatus (SHEILA) described in this paper. SHEILA was built as a first prototype with the limited aims of demonstrating the existence of closed magnetic surfaces in this configuration and of comparing, if possible, the magnetic field geometry actually produced with that predicted by numerical calculation. Despite the small size of the apparatus, it has also been possible to perform several experiments on the properties of the plasma produced in and confined by its magnetic fields.

The apparatus was originally designed and constructed with no helical control winding, and therefore with an essentially fixed magnetic configuration. The initial experimental results verifying the existence of a low-pressure equilibrium in this apparatus were reported briefly in 1985 (Blackwell *et al.* 1985). A helical control winding was added during 1986, and the preliminary results of its effect on plasma formation and confinement reported to the IAEA plasma physics conference later that year (Blackwell *et al.* 1987).

The main apparatus is described in the next section. The range of possible magnetic configurations and their computation are discussed in Section 3, and some detailed examples given. The measurement techniques are outlined in Section 4, and some illustrative experimental results presented and discussed in Section 5. Finally a brief comment is made about the extension of this work to a much larger apparatus (H-1) now under construction.

For the benefit of those unfamiliar with the stellarator geometry, some definitions, etc., are given in an Appendix.

## 2. Apparatus

The construction of the SHEILA apparatus is shown in Fig. 1: because of successful experience with PROTO–CLEO (Bolton *et al.* 1971) and TORSO (Hamberger *et al.* 1975) it was decided to locate the magnetic coils inside a cylindrical stainless-steel vacuum tank and to allow the plasma boundary

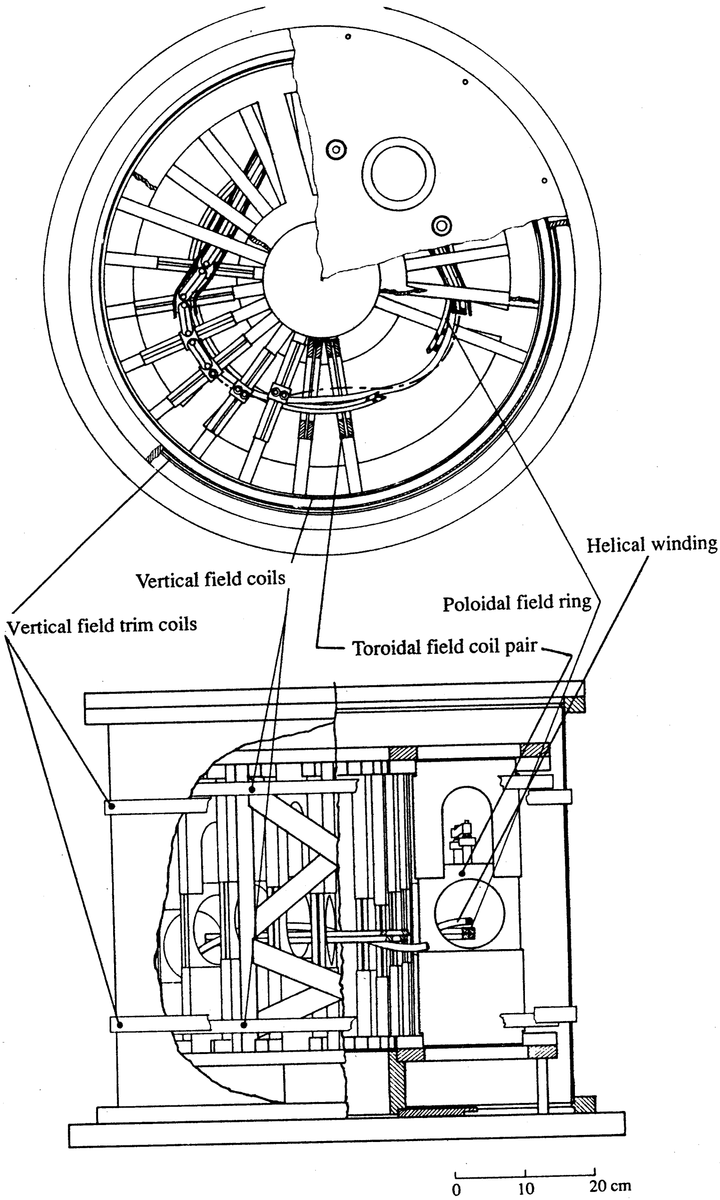


**Fig. 1.** The SHEILA heliac, showing the magnetic field coils as labelled, the support structure, vacuum vessel and current feeders; see also Fig. 8.

to be defined by the outermost closed magnetic surface. The tank, which is approximately 650 mm in diameter and 600 mm high, can be fitted with an alternative transparent polycarbonate lid for visual observation purposes, at the expense of vacuum quality.

The main toroidal field is provided by 24 two-turn coils (Fig. 2), made from radially split, 150 mm square, 6 mm thick copper plates with 110 mm circular

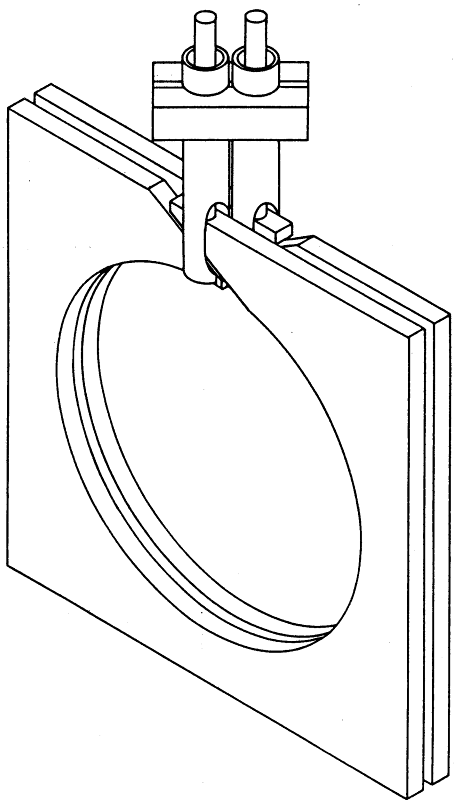

**Fig. 2.** Toroidal field coil pair with current feeds joined by a connecting block. Stray fields are reduced by the planar and coaxial current paths, and the antisymmetry of the pair.

apertures. These are mounted in parallel pairs inside insulated box section extensions made from 1·2 mm thick stainles-steel sheet, which in turn are supported vertically between upper and lower radial arms spaced at 15° intervals around the azimuth so that the mid-plane of each coil pair is radial. The height and horizontal position of each coil pair can be adjusted so that the centre of the pair lies on some given toroidal helix which is (usually) centred on the circle which forms the minor axis of the machine ($R_0 = 187\cdot 5$ mm) and displaced from it by a distance $\rho_s \leq 50\,mm$. The arrangement allows various helices to be employed, according to the general law $\theta = N\phi + \alpha \sin N\phi$, where $\theta$, $\phi$ are the usual poloidal and toroidal angles, $\alpha$ is a constant, and the number of field periods $N$ can, in principle, be chosen as 1,2,3,4,6 or 8. In practice, the helix has been kept fixed with parameters $N = 3$, $\rho_s = \mathrm{const.} = 25$ mm, $\alpha = 0\cdot 1$, which approximates to the form of the first Princeton reference design (T. K. Chu, personal communication 1983). The main magnetic and plasma parameters of SHEILA are shown in Table 1.

The poloidal field coil consists of four turns of square-section copper (7 mm×7 mm) machined from plate and insulated from each other by 0·4 mm thick, vacuum quality epoxy resin ('torseal'). The ring is supported from below so that its centre line coincides with the minor geometric axis. The helical winding is a single copper conductor of 6 mm diameter circular cross section closely wound three times around the poloidal field coil in phase with the helix followed by the toroidal coil centres. The mean radial excursion of the helix

**Table 1. Magnetic and plasma parameters of SHEILA compared with the heliac H-1 currently under construction**

| | SHEILA | H-1 |
|---|---|---|
| $B_0$ (T) | 0·2 | 1·0 (0·25 continuous) |
| Pulse duration (s) | 0·04 | 1 |
| Field periods $N$ | 3 | 3 |
| Number of TF coils | 24 | 36 |
| Major radius (m) | 0·1875 | 1 |
| Average minor radius (m) | 0·035 | 0·2 |
| Swing radius $\rho_s$ (m) | 0·025 | 0·22 |
| Transform $\iota$ | 0·7–2 | 0·8–1·8 |
| $\iota(0)$, at $I_h/I_r = 0$ | 1·187 | 1·09 |
| Well at $I_h/I_r = 0$ | 3·6% | 5% |
| Shear | −0·05 to 0·2 | −0·1 to 0·15 |
| RF heating power | 400 W | 200 kW |

is 14·3 mm. Finally, the vertical field needed to complete the configuration is produced by two single-turn coils of radius 313 mm, located 192 mm above and 145 mm below the median plane, plus two further single turns of radius 334 mm, located 199 mm above and 127 mm below the median plane, this time outside the vacuum vessel, and used for fine adjustment of the vertical field.

Considerable care has been taken in the design of the current feeds and inter-coil connections in order to minimise the effects of their magnetic fields on the magnetic surfaces. These include, for example, the use of coaxial connectors to feed each turn of each toroidal field coil, the manner in which the feeders are connected to the coils, and the use of a three-element, parallel plate transmission line between the feeders. However, a deliberate decision was made to use normal workshop tolerances throughout fabrication and assembly in order to test the robustness of the configuration: the overall positional accuracy of the toroidal field coils has been measured at (±0·5 mm, ±0·3 mm) random, (+1·5 mm, +2 mm) systematic for $(R,Z)$ and the ring core and inner VF coils ±2 mm. These measurements were made *in situ* after three years of operation, and are not as precise as the measurements made at the time of manufacture which showed greater positional accuracy.

In order to maintain the magnetic geometry constant when operating from the pulsed power supplies, all coils are operated in series, where necessary using shunts with matched time-constants to vary the ratios of currents. The use of shunts requires further that mutual inductance between the winding being shunted and other parts of the circuit be cancelled. This is particularly important with regard to the sharing of the toroidally directed currents between the poloidal field and helical coils, and for this purpose, a small air-cored transformer is used, constructed in two matched halves oriented to cancel the magnetic dipole moment of the transformer. Once the currents are distributed in the correct ratio the magnetic configuration remains essentially fixed at all times during a given pulse, although some time dependence is detectable and is allowed for in cases where the configuration depends critically on the currents (for example when $\iota \sim 3/2$).*Thelowimpedanceloadpresented*

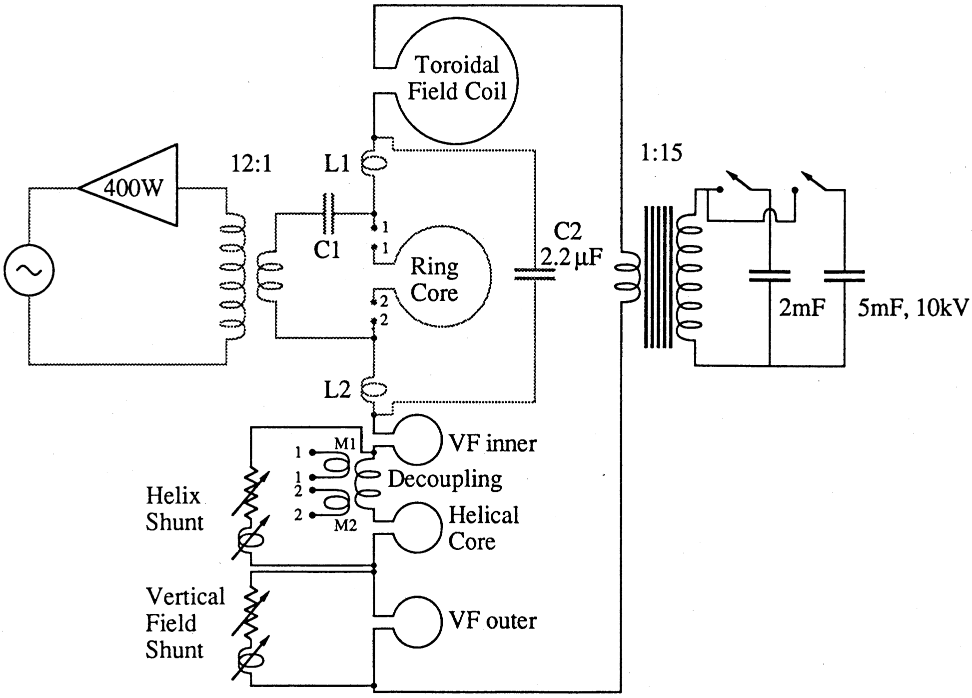


**Fig. 3.** Simplified circuit for the SHEILA magnetic field power supply (solid) and RF power supply (dotted). C1 and the ring core form a resonant circuit, L1 and L2 are RF isolation chokes, and M1 and M2 cancel the mutual inductance between the ring core and helical winding.

by the coils is powered from two capacitor banks (2 mF and 5 mF, 10 kV max.) which can be fired singly, together, or sequentially, matched by a 15 : 1 iron-cored step-down transformer (biassed to provide a maximum flux swing 0·2 Wb). The arrangement produces current pulses with rise times of 7–10 ms and maximum duration up to 40 ms with peak fields ($B_0$) up to 0·38 T (at 7 kA). Direct measurements confirm that the current rise is sufficiently slow that within the plasma volume the effects of induced eddy currents in the apparatus can be ignored.

The electrical circuit is shown schematically in Fig. 3, with the effective RF path (Section 4) indicated by dotted lines.

## 3. Magnetic Field Configurations

As indicated earlier, the magnetic field lines trace out and lie on topologically toroidal surfaces whose axis rotates three times around the central conductor in one toroidal turn, each poloidal rotation thus representing one of three nominally identical field periods. The detailed geometry of the surfaces themselves and of their associated field lines depends on the particular distribution of currents in the various windings, as well as those self-consistent currents within the plasma required to balance its kinetic pressure. For the purposes of this paper we can safely ignore the effect of plasma currents since, under all plasma conditions relevant to this work, the pressure is sufficiently low.

The magnetic surfaces are calculated numerically by now well-established procedures (Gibson 1967; Ehrhardt 1985; Blackwell 1988) in which the coil currents are represented by a sufficient number of filamentary currents, and their resultant magnetic field vector calculated and followed for many toroidal rotations. By exploring all relevant regions of space one can find all possible magnetic surfaces which can be formed free of physical obstruction. Provided sufficient accuracy is maintained the procedure also provides the necessary information to derive the important quantities which determine the macroscopic plasma behaviour, such as rotational transform, magnetic well and, to first order in $\beta$ (the ratio of plasma to magnetic pressure), the distribution of pressure-driven currents.

In these calculations the coil currents have been approximated entirely by circular current filaments distributed as follows: for the toroidal coil set by three equal filamentary currents ($\frac{1}{3}I_0$ at radii 58·2, 64·6 and 71·0 mm) in each of the 48 copper plates, centred and oriented as constructed; the poloidal ring by one filament at the centre of each of its four turns, carrying current $I_0$ ($I_r \equiv 4I_0$); the helical winding by a single filament ($I_h$)of winding law $R = R_0 + \rho_h \cos N\phi$, $z = \rho_h \sin N\phi$, where $\rho_h$ is the radius with respect to the minor axis; and by one filament at the centre of each vertical field coil ($-I_0$ for inner coils and typically $-0 \cdot 21 I_0$ for outer coils).

For the purposes of illustration, we present first the results of such a calculation for a carefully optimised set of coil current conditions for which the helical winding current is $I_h = 0$, and which we refer to as the 'standard' case. Shown in Fig. 4 are the cross sections of several computed vacuum surfaces at two phases ($\phi = 120°$ and $60°$) within one helical field period. For convenience we label each flux surface by a parameter $X$ taken as the horizontal distance (in cm) measured radially outwards from the magnetic axis ($X = 0$) in the plane $\phi = 0$ (see the Appendix).

The outermost surface shown ($X = 2 \cdot 0$) has a mean radius $a$ (defined by the cross-sectional area $\pi a^2$) of approximately 31 mm. The rotational transform $\iota$ on this surface is 1·35, compared with 1·18 on the magnetic axis.

The variation of rotational transform $\iota(X)$ together with that of the specific flux volume $V'$ (magnetic well—see Appendix) is shown in Fig. 5 for the standard case. As can be seen, the $V'$ dependence corresponds to the existence throughout the plasma volume of a magnetic well ($V'' < 0$) which reaches a maximum depth of about 4% on the axis.

Such magnetic surfaces can be seriously disturbed by resonant interaction with perturbing magnetic fields (whether internally or externally caused) of the form $\Sigma B_{m,n} \cos(m\vartheta - n\phi)$ when the helical transform (see Appendix) is resonant ($\iota = n/m$). Since, in general, the harmonic amplitudes $B_{m,n}$ decrease with increasing $m$ and $n$, low order resonances are to be avoided. In this example the lowest order resonances with symmetrical error fields occur for $\iota = 6/5$, near the axis, and $\iota = 9/7$, towards the outside, and for non-symmetrical error fields, $\iota = 5/4$. The symmetry-breaking $\iota = 1/1$ resonance, although outside the range of rotational transforms in the standard case, makes the configuration quite sensitive to alignment of the ring core and the toroidal field coil set. For example, a 1·5 mm displacement of the ring core was found to cause movement in the magnetic axis position of up to four times this amount for the standard case,

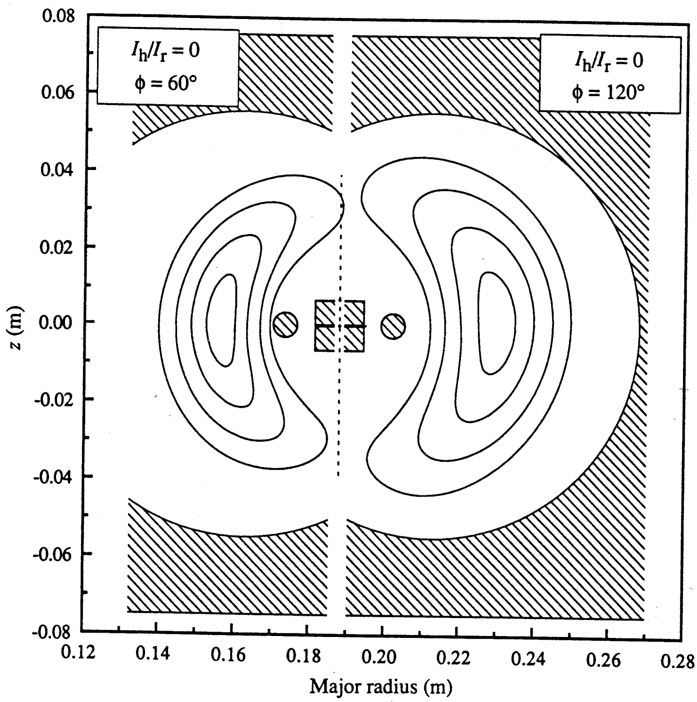


**Fig. 4.** Magnetic surfaces for $I_h/I_r = 0$ showing sections at two toroidal locations ($\phi = 120°, 60°$).

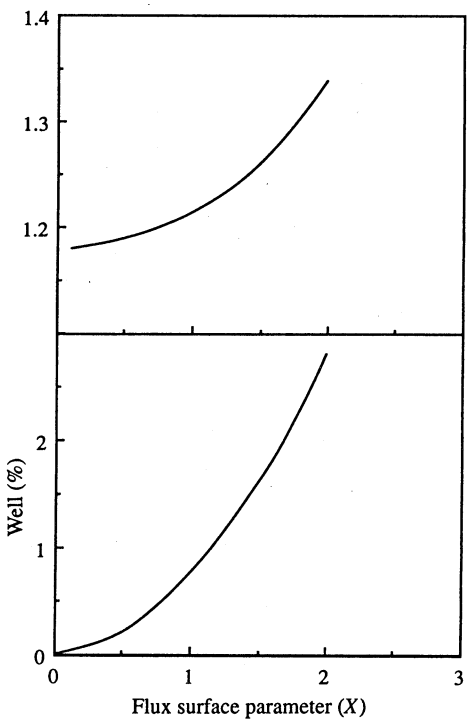


**Fig. 5.** Computed rotational transform $\iota$ and magnetic well for $I_h/I_r = 0$.

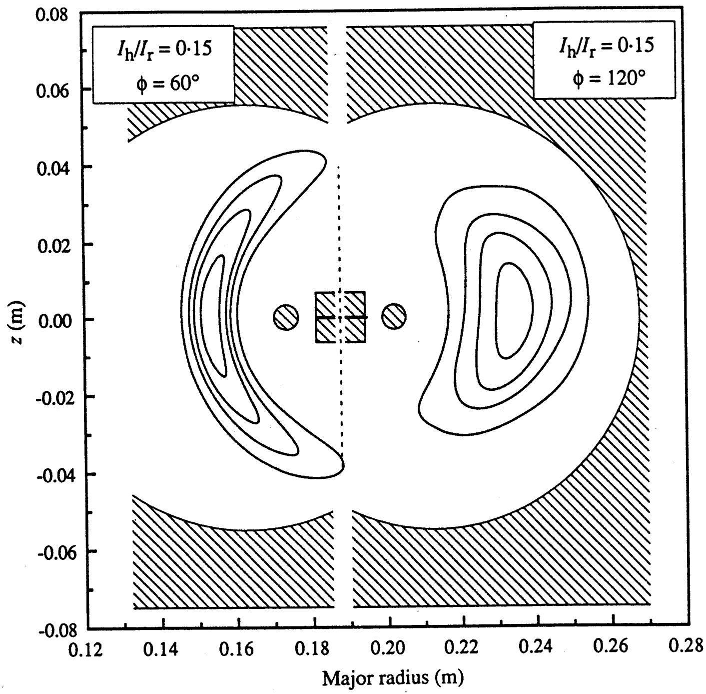


**Fig. 6.** Magnetic surfaces for $I_h/I_r = 0 \cdot 15$.

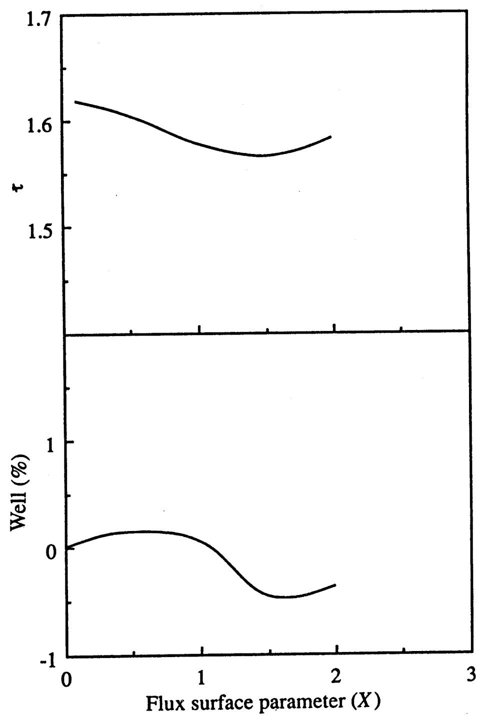


**Fig. 7.** Computed rotational transform $\iota$ and magnetic well for $I_h/I_r = 0 \cdot 15$.

and had even greater effect, when the $\iota = 1$ surface is near the magnetic axis ($I_h/I_r = -0 \cdot 05$) (Shi *et al.* 1988).

Fig. 6 shows surfaces for a different magnetic configuration in which a current of $0 \cdot 15 I_r$ flows in the helical core, in the same sense as $I_r$. The rotational transform is higher ($\iota = 1 \cdot 6$, see Fig. 7), being this time above the 3/2 resonance, and varying little with radius. The magnetic well is virtually non-existent, the area of the surface at $\phi = 120°$ is reduced, and the surface at $\phi = 60°$ is elongated.

## 4. Plasma Production and Measurements

The vacuum system is evacuated to a base pressure of $<2 \times 10^{-6}$ Torr (1 Torr ≡ 133 Pa) by an oil ('Santovac V') diffusion pump fitted with a refrigerated baffle. Various gases, usually hydrogen, helium or argon, are introduced at a constant rate to provide filling pressures in the range $10^{-5}$–$10^{-3}$ Torr. Discharges are obtained by superimposing a small oscillatory current (about 100 A turns at frequencies 100–300 kHz) upon the slowly varying and much larger currents in the poloidal field ring (typically 16 kA turns). The oscillatory current is derived from a solid-state amplifier producing up to 400 W output power, and supplied through appropriate capacitors to the ring, forming a series resonant circuit. The arrangement induces a loop voltage $\leq 17$ V r.m.s. at the magnetic axis, which is sufficient to produce an oscillatory discharge within the closed toroidal surfaces by long-path breakdown (Section 5.1). The discharge persists as long as the RF power is applied, provided the magnetic field exceeds about $0 \cdot 05$ T. Since the presence of plasma both loads and detunes the resonant circuit, the frequency is adjusted when necessary by pre-programming the oscillator driving the amplifier. Because plasmas produced in this way typically have electron densities $n_e$ and temperatures $T_e$ in the ranges $10^{17} < n_e < 10^{19}$ m$^{-3}$ and $T_e \leq 13$ eV respectively, and last only 10–20 ms, they are amenable to relatively simple Langmuir probe techniques provided proper precautions are taken.

The greatly reduced symmetry of the heliac configuration compared with, for example, a tokamak leads to the necessity of exploring virtually the whole region inside the outermost closed flux surface, rather than being able to rely on measurements along only one or two chords. To achieve the necessary coverage, the apparatus is equipped with horizontally movable probes which can be inserted in 10 ports distributed around the torus: in addition at two locations, corresponding to $\phi = 120°$ and $\phi = 150°$ in Fig. 8, probe arrays consisting of seven probes can be pre-set to sample any given magnetic surface; and one probe whose tip can be accurately located at any point within a plasma cross section is controlled from outside the vacuum vessel by means of a mechanical linkage (Fig. 9).

Each Langmuir probe consists of a $0 \cdot 3$ mm (or 1 mm) diameter tungsten wire sheathed in fused silica with a 2 mm long exposed end as a collector. Provided care is taken to clean the probe surface (using a 30 A m$^{-2}$ glow discharge in argon at $0 \cdot 6$ Torr for 5 minutes) the characteristics obtained are quite reproducible. The analysis of the data to obtain electron temperature and density under the prevailing conditions (long mean-free-path, strong magnetic field, etc.) is made

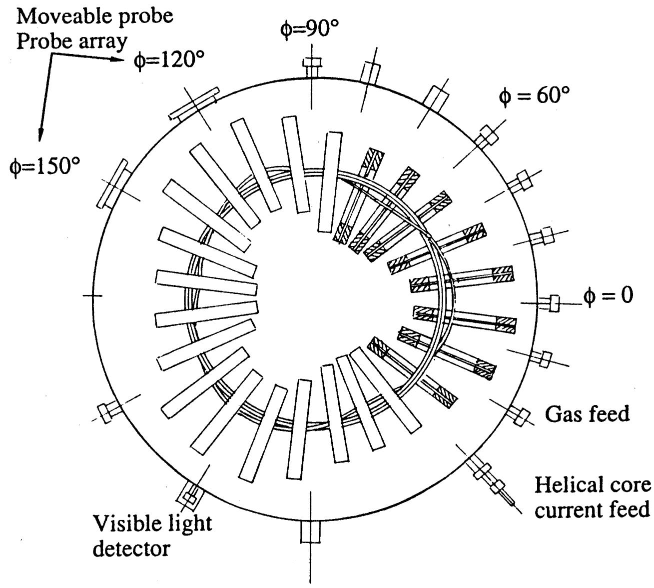


**Fig. 8.** Plan view of SHEILA showing the port locations relative to the helical core for measurements referred to in the text. The plasma follows the same winding law as the helical core. Some components of the machine not visible in Fig. 1 are shown.

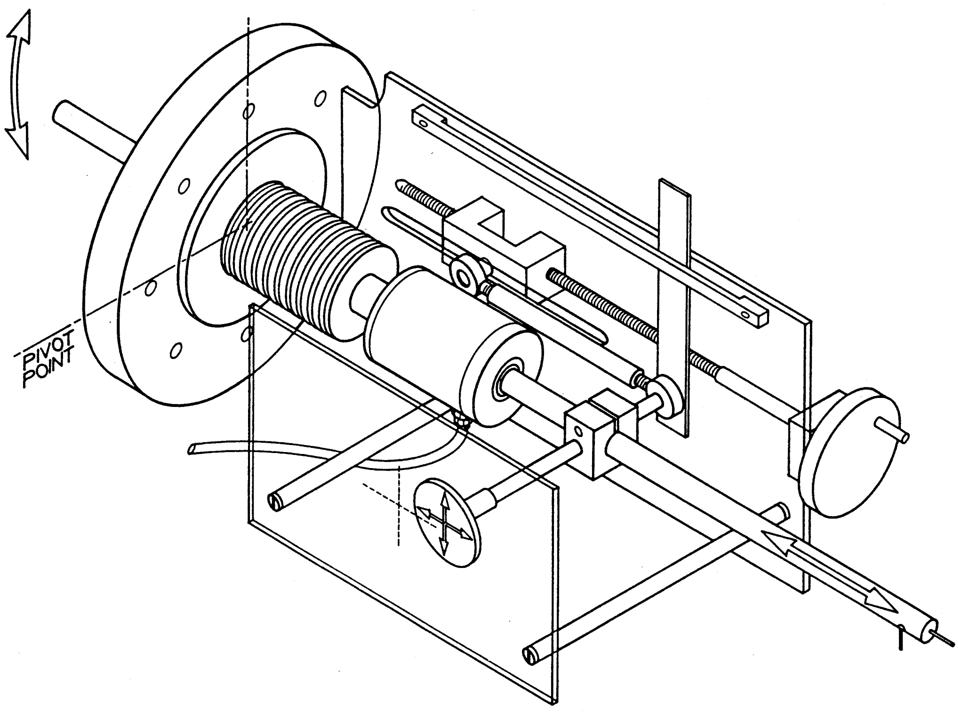


**Fig. 9.** 2D probe positioner. Independent control over probe insertion depth and angle allow the entire plasma cross section to be scanned through a small port. A pivot and lever arm system allows the probe motion to be tracked externally on a surface cross section map with only mild geometric distortion, allowed for in the map.

following Swift and Schwar (1970). For those conditions in which the electron temperature remains fairly constant, the electron density can be simply related to the saturated ion current to the probe. The probe calibration has been confirmed by comparison with the interferometer measurements.

The other diagnostic techniques used include a 2·2 mm wavelength microwave interferometer, which measures line integrated electron density from the phase shift produced in two passes along a chord; small magnetic probes used to explore fluctuations of the magnetic field; visible light emission as a crude measure of ionisation rate; and Rogowski coils to measure axial plasma current.

Signals from the various diagnostics are usually recorded digitally for subsequent analysis using the data acquisition system developed for the LT-4 tokamak (Courbould and How 1984). Typical waveforms are shown in Fig. 10.

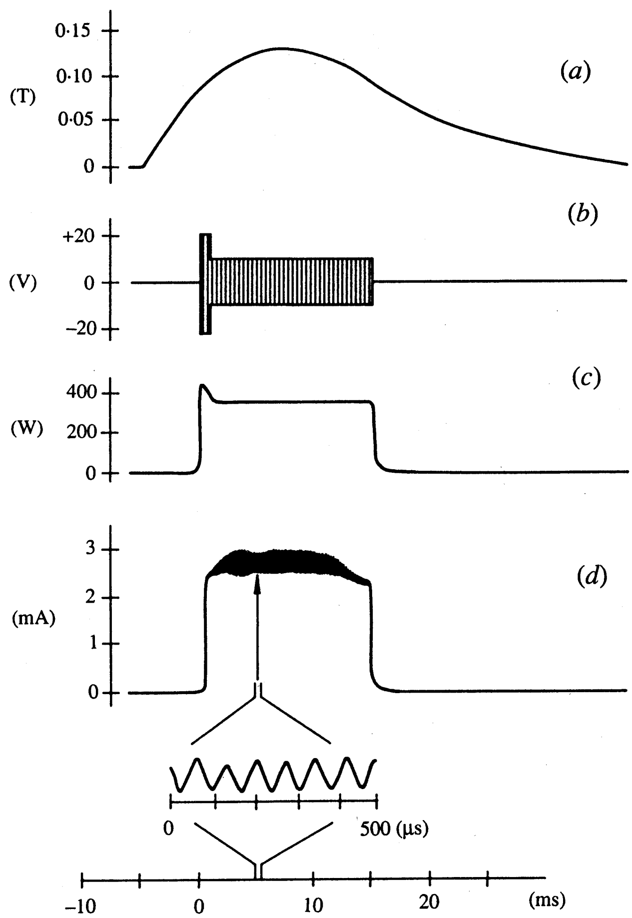


**Fig. 10.** Typical waveforms: (*a*) mean magnetic field strength; (*b*) envelope of RF voltage per turn at the ring conductor; (*c*) DC power input to RF amplifier; (*d*) ion current to probe biassed to −90 V at $X = 1 \cdot 0$, $\phi = 120°$ (1 mA corresponds to $n_e = 4 \times 10^{17}$ m$^{-3}$ at $T_e = 6$ eV).

## 5. Principal Results

### *5.1 Breakdown and Plasma Properties*

The oscillatory current in the ring induces an electric field in the range $E_\phi < 12\,\mathrm{V\,m^{-1}}$ r.m.s., which accelerates free charges along the lines of the confining magnetic field. Breakdown occurs for electric fields above some critical value, and a small oscillatory current is set up which ohmically heats the resulting plasma. At the time of peak magnetic field, the small loop voltage $\leq 0\cdot1$ V/turn induced by the changing flux, generated by the slowly varying current in the ring, would also cause a small current (~ 15 A) to flow in the conducting plasma. Careful measurements of this current, using one circular Rogowski loop encircling the plasma and the central ring, in series with a second identical Rogowski loop monitoring four turns of the power supply current to subtract the contribution from the ring current, establish an upper limit on this current of 40 A. It should be noted that such a small current can be ignored both in terms of its contribution to the magnetic field and to the plasma heating.

Preliminary experiments (Conway 1988) with a 2·45 GHz, 600 W source indicate that a microwave generated plasma may be obtained at the electron cyclotron resonance ($B$_0 ~ 0·095)with parameters similar to those of the plasma generated by the method just described.

*5.1.1 Breakdown Threshold.* The electric field at the onset of breakdown was measured in the standard configuration ($I_\mathrm{h} = 0$) for various gases, filling pressures, confining magnetic field strengths and frequencies $\omega_0$ of the applied electric field. The measured breakdown field is shown in Figs 11*a* and 11*b* plotted against gas pressure for hydrogen and argon at two different frequencies. It can be seen that the minimum electric field corresponds to the condition $\nu_\mathrm{m} \approx \omega_0$, where $\nu_\mathrm{m}$ is the electron–neutral collision frequency for momentum transfer (Blackwell and Shi 1988). In Fig. 12, we use the constant collision frequency assumption (Allis and Brown 1952) (for an energy near the ionisation energy) by plotting an effective electric field

$$E_\mathrm{eff} = E\left(\frac{\nu_\mathrm{m}^2}{\nu_\mathrm{m}^2 + \omega_0^2}\right)^{\frac{1}{2}} .$$

Collision frequencies of the form $\nu_\mathrm{m} = 5\cdot9\times10^9 p(\mathrm{Torr})$ and $\nu_\mathrm{m} = 1\cdot3\times10^{10} p$ were used for the hydrogen and argon data respectively to enable comparison with the data from Brown (1959). All the data for both gases and both frequencies were then reduced to lie within ±20% of a single curve, supporting the validity of the collision frequency dependence. The frequency dependence in the present hydrogen data was more effectively removed (Blackwell and Shi 1988) by choosing a smaller $\nu_\mathrm{m}$, which is consistent with recent cross-section data (Shyn and Sharp 1981). More detailed analysis, requiring knowledge of the electron energy distribution function (MacDonald 1966), is beyond the scope of this paper.

The conditions here are markedly different from those under which RF breakdown phenomena have been previously studied (Brown 1959). The

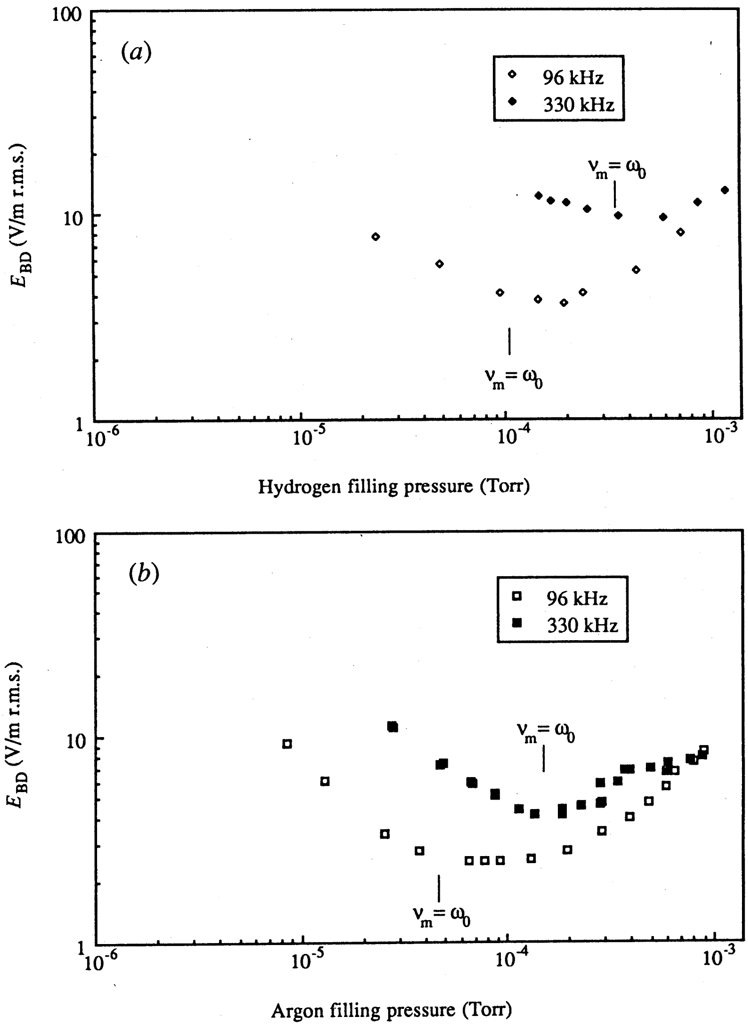


**Fig. 11.** Breakdown toroidal electric field $E_{BD}$ for different excitation frequencies and pressures: (*a*) hydrogen; (*b*) argon.

electron collision mean-free-path is much larger, and the magnetic field is highly non-uniform. However, it is noteworthy that the general behaviour shows strong similarities to the results obtained in situations where the charge loss processes can be well described by collisional diffusion. The diffusion interpretation is supported by preliminary measurements of the dependence in $B_0$ (Blackwell and Shi 1988). The breakdown curve shown in Fig. 12 could be regarded as an extension of the corresponding curves of Brown (1959, see e.g. Fig. 5.5a) to much lower pressures, provided that the value of the characteristic diffusion length is taken to be in the range $\Lambda \sim 2$–$10$ m. This is much shorter than lengths obtained from electron orbit calculations or from simple collisional diffusion, but we have not considered here the rather

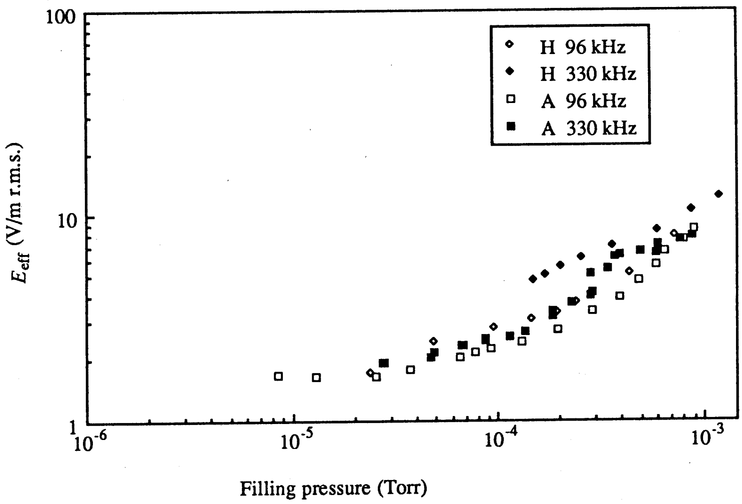


**Fig. 12.** Data of Figs 11*a* and 11*b* replotted as $E_{\mathrm{eff}}$ (see Subsection 5.1.1).

complicated effects of trapped particle drifts, which are at present under investigation.

The variation of breakdown electric field with rotational transform is shown in Fig. 13*b*. Near the $\iota/N = 1/3$ and $1/2$ resonances, plasma formation becomes more difficult until, at $\iota/N \sim 1/3$, plasma could not be formed. Both cross-field diffusion and the effect of error fields should be considered in the interpretation of this result. Near the $\iota/N = 1/3$ resonance, particles are no longer forced to sample the entire plasma volume, and stray fields (electric or magnetic) can more readily induce particle drift. Away from low order resonances the surfaces are closed, but the shape changes (see inset), and if a surface becomes narrow at any value of $\phi$, particles can more readily escape from the plasma core.

*5.1.2 Plasma Density.* The plasma density depends primarily on the amplifier output power and the filling pressure, as shown in Fig. 14. Fractional ionisations near unity (dotted line) are possible in argon, considerably less for helium and hydrogen. The plasma density would also be expected to mirror the particle confinement time, and this is demonstrated in a configuration scan (Fig. 13*a*), obtained by varying the current in the helical control winding. The dependence is qualitatively the inverse of the breakdown electric field dependence, as discussed in Subsection 5.1.1.

## *5.2 Equilibria*

An essential property of a toroidal equilibrium is that the kinetic pressure $p$ of the plasma confined by the magnetic field depends only on the local value of the toroidal flux function $\psi$; since by definition $\psi$ is constant on a given flux surface, $p$ must be a function only of $\psi$, i.e. $p$ is constant on any given flux surface. Hence, an experimental demonstration that $p = \Sigma n_j T_j \sim n_e T_e$ is the same at all accessible points on a predicted surface may be taken as evidence that those surfaces do exist as calculated.

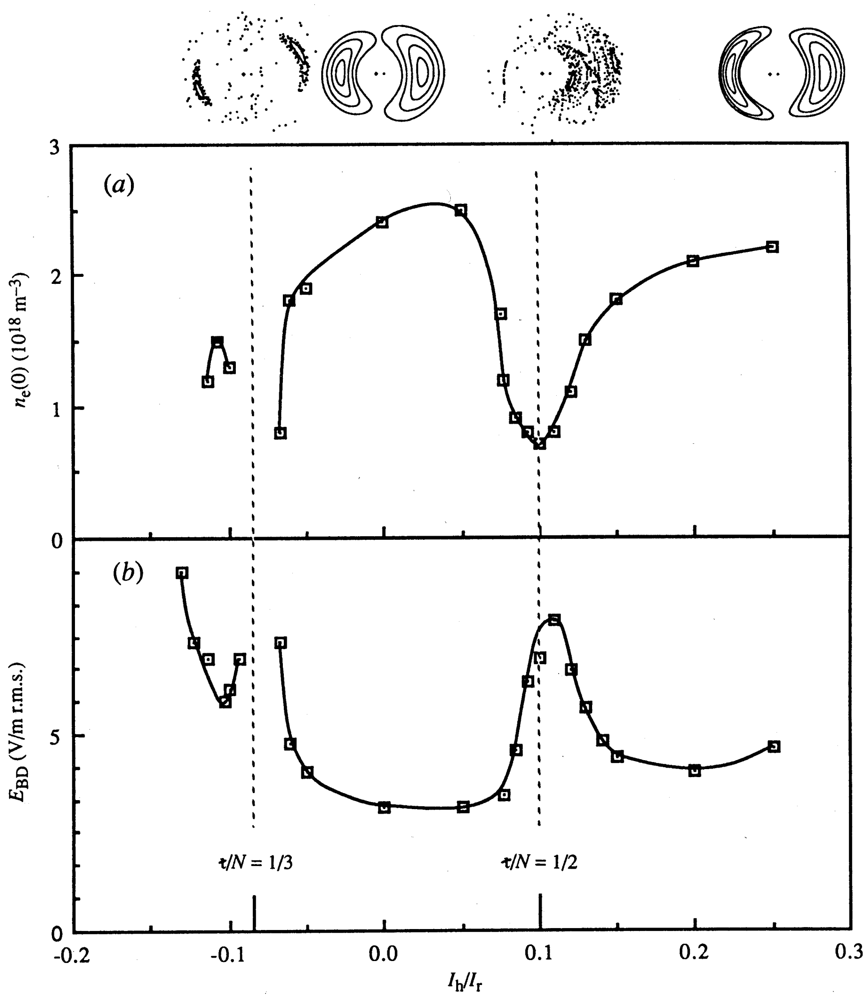


**Fig. 13.** Variation of (*a*) central plasma density and (*b*) breakdown toroidal electric field with helical core current. As the ratio $I_h/I_r$ is varied, the configuration changes considerably as shown in the top inset. Most configurations are nested surfaces, but surface breakup occurs in narrow bands near $ɫ/N = 1/3$ and 1/2 as illustrated.

At the simplest level, the existence of a helical plasma column formed in the magnetic fields by the discharge can be demonstrated by photographs such as that reproduced in Fig. 15: the luminous region is clearly restricted to inside the outermost flux surface. More precise information can be obtained by making chordal scans of the electron density and temperature using Langmuir probes and relating their product $p = n_e T_e$ at each point to the particular flux surface $X$ on which the point lies. To do this we rely on the fact that the plasma pressure is sufficiently low compared with that of the magnetic field so that it is sufficient to calculate the vacuum magnetic field, i.e. due to the currents in the external conductors alone since the self-consistent current

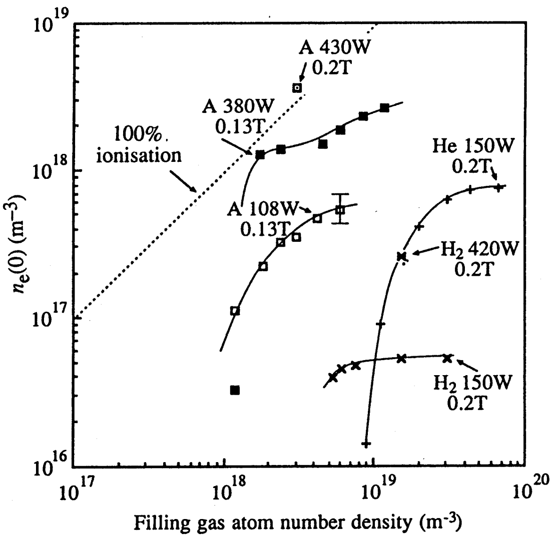


**Fig. 14.** Range of discharges obtained in SHEILA for various filling gases (A, H, He), filling pressures (expressed as atom number density), and RF amplifier powers. At lower plasma densities, only a small fraction of the power available is absorbed by the plasma.

induced in the plasma to balance its pressure is very small. Examples obtained for the 'standard' configuration ($I_h = 0$) of chordal variations of $n_e$, $T_e$ and $n_e T_e$ are shown in Fig. 16 for two horizontal scans, one through the horizontal mid-plane at $\phi = 120°$ (where the plasma lies outside the ring) and one at $\phi = 60°$ (plasma inside the ring). The outer surface cross section and chordal paths explored by the probe are shown in the inset. The chordal variations clearly reflect the shape of the surfaces.

Fig. 17 now shows the same data plotted as a function of the flux surface parameter $X$ corresponding to the probe location, where $X$ has been obtained by computation of the fields due to the *actual* currents used in the experiment. It can be seen that, regardless of actual position, the data all fit well to a single curve, $p = p(X)$, with (as expected) maximum pressure on the axis decreasing to a much lower value at the last closed surface which can be identified (see the Appendix).

For the case $I_h/I_r = 0 \cdot 15$, the two radial scans are more clearly different (Fig. 18), but the variation between cross sections is still small (Fig. 19), less than 10% of the central value.

### 5.3 *Plasma Fluctuations*

Under most conditions the saturated ion currents to the Langmuir probes show fluctuating signals, with frequencies typically in the range 10–100 kHz (depending on the filling gas), and relative amplitudes $\delta n_e/n_e \sim 0 \cdot 01$–$0 \cdot 3$. The associated magnetic field fluctuations are found to have essentially the same spectrum, but considerably reduced amplitude relative to $B$.

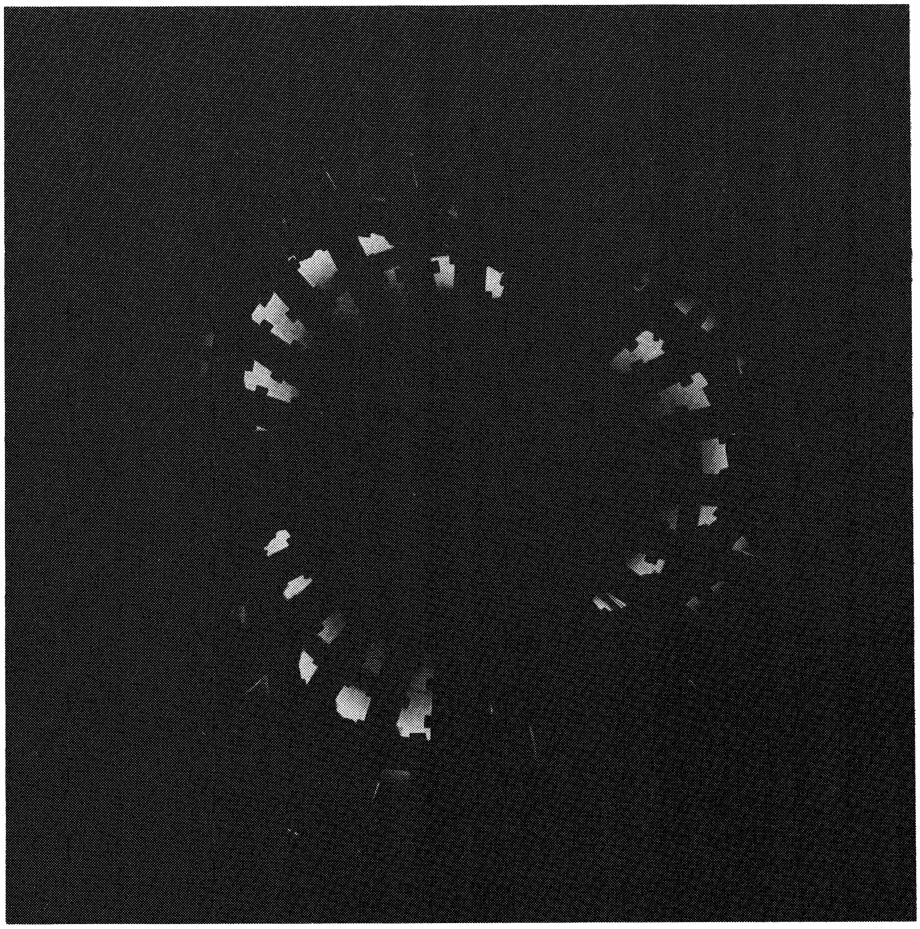

**Fig. 15.** Photograph taken from above through a transparent polycarbonate lid, showing the luminous argon plasma encircling the ring core three times. The toroidal coil current feeder transmission line system (Fig. 1) blocks the plasma light along a path that closely follows the plasma axis.

To an order of magnitude, we find that

$$\frac{\delta B}{B} \sim 10^{-5} \frac{\delta n_e}{n_e}.$$

This is consistent with the nature of the fluctuation being predominantly electrostatic, rather than magnetohydrodynamic, with the local magnetic field oscillations arising only from the plasma pressure oscillations, i.e.

$$\frac{B^2}{2\mu_0} + n_e T \sim \text{const.}, \qquad \frac{\delta B}{B} = -\frac{1}{2}\beta \frac{\delta n_e}{n_e},$$

where $\beta = 2\mu_0 nT/B^2 \sim 10^{-5}$ for our conditions near the edge of the plasma where the oscillation is most obvious.

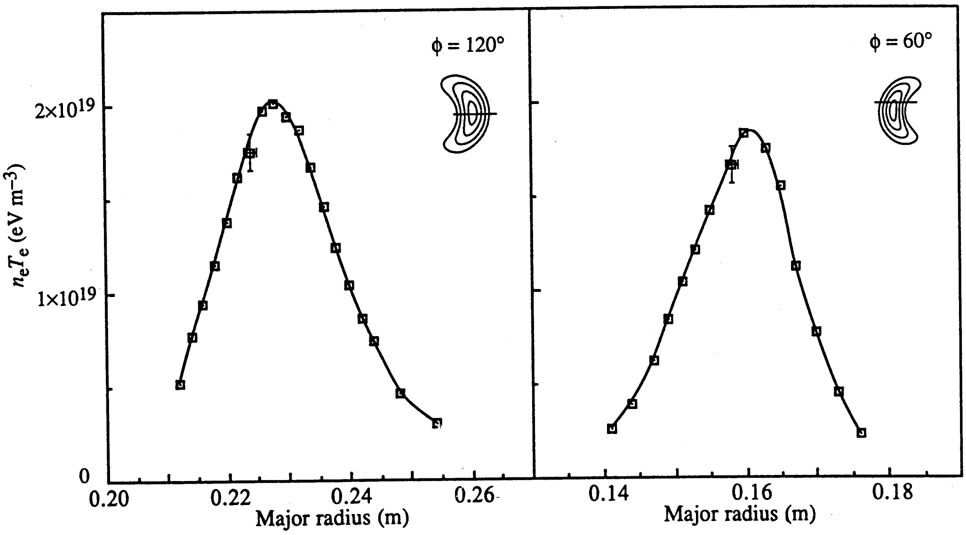


**Fig. 16.** Plasma pressure deduced from probe measurements along the chords shown (inset) at $\phi = 120°$ and 60°, with no helical core current ($I_h/I_r = 0$).

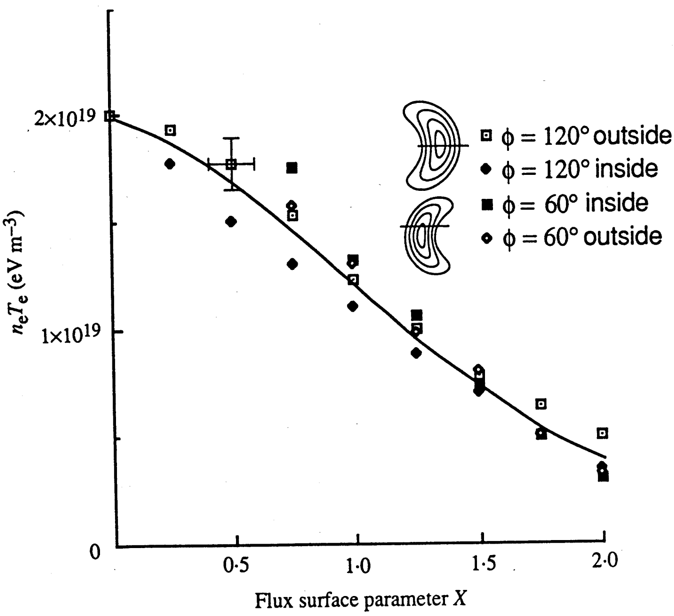


**Fig. 17.** Data of Fig. 16 re-plotted as a function of the flux surface parameter $X$.

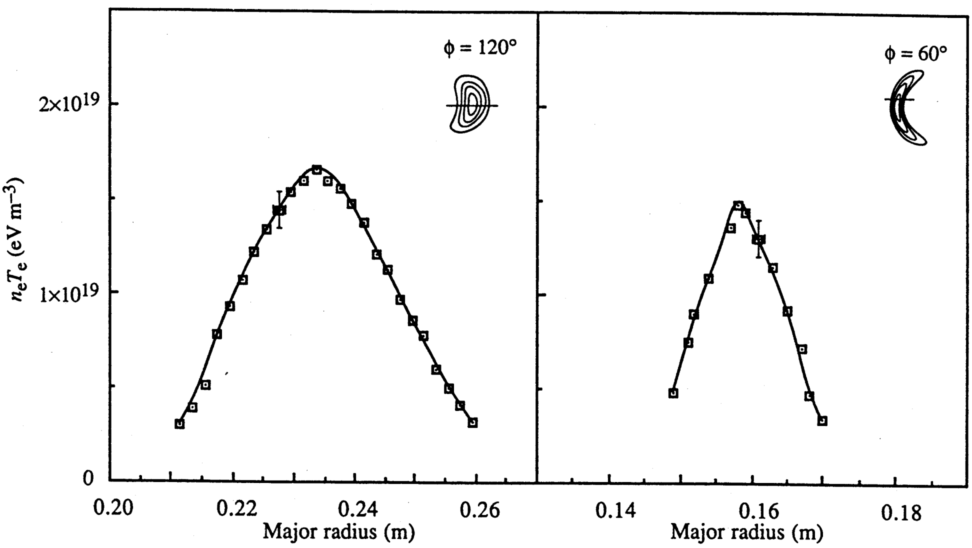


**Fig. 18.** As for Fig. 16, but with helical core current ($I_h/I_r = 0\cdot15$).

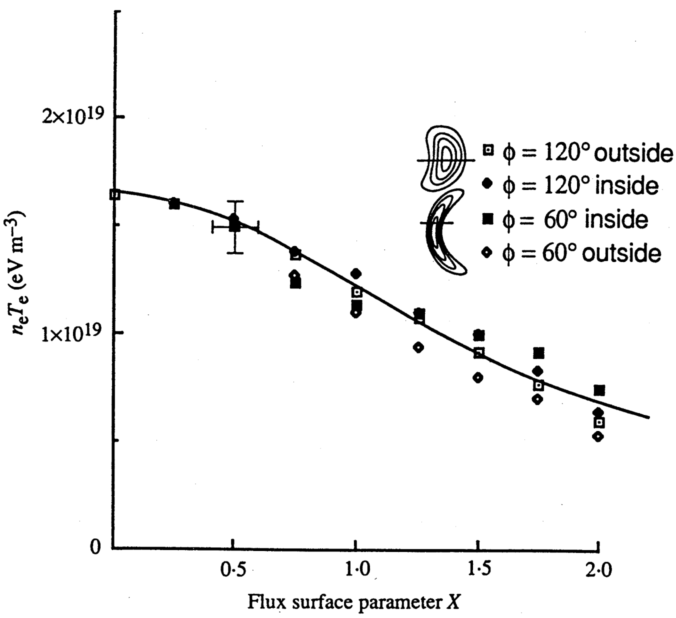


**Fig. 19.** Data of Fig. 18 reduced as in Fig. 17.

**Table 2. Threshold fields for a range of experimental conditions**

| Species | $B_{\mathrm{thr}}$ (T) | $M_i^{1/2}$ | $\rho_i/a$ |
|---|---|---|---|
| $H_2$ | 0·021 | 1·0 | 0·37 |
| He | 0·042 | 2·0 | 0·34 |
| A | 0·12 | 6·3 | 0·34 |

*5.3.1 Fluctuation Threshold.* The fluctuations appear only when the applied magnetic field $B$ exceeds some threshold value which depends mainly on the ion mass $M$. Table 2 shows the threshold fields for a range of experimental conditions. The last column shows the ratio $\rho_i/a$, where $\rho_i = (T_e M)^{1/2}/eB$ is the effective ion Larmor radius, and is consistent with the threshold condition: $\rho_i/a \approx \text{const.} \approx 0 \cdot 4$. This suggests that the observed fluctuations have the form of self-excited electrostatic drift modes, since these are restricted to wavelengths $2\pi/k_\perp$ perpendicular to $\boldsymbol{B}$ such that $k_\perp \rho_i \leq 1$, with the most unstable modes having $k_\perp \rho_i \sim 0 \cdot 3$–1.

*5.3.2 Steady-state Fluctuations.* As the threshold is exceeded, the fluctuation first appears as a single, coherent mode, then loses coherence as $B$ increases until, for sufficiently small $\rho_i/a$, the spectrum becomes turbulent. When only a single coherent mode is present it becomes relatively simple to study its eigen-structure by making simultaneous direct measurements of its amplitude and phase at multiple locations within the plasma, using the probes described in Section 4. Since it is expected that such electrostatic drift modes would have their wave-vectors aligned almost perpendicular to the magnetic field ($\boldsymbol{k}.\boldsymbol{B} \sim 0$), it is convenient to refer the measurements to a coordinate system $(X, \vartheta, \phi)$ in which the field lines appear to be straight (see the Appendix), with $X$ serving as a flux coordinate in place of the minor radius, i.e. in the form $\xi = \xi(X) \exp\{i(m\vartheta - n\phi)\}$.

Figs 20–22 show the results obtained for the 'standard' configuration ($I_h = 0$) using argon plasma. The variation of amplitude and phase with $X$ in Fig. 20 shows that the fluctuation is in the lowest 'radial' eigenmode with a maximum amplitude $\delta n/n$ near the outer edge of the confined region of plasma. In Fig. 21 the variation of phase and amplitude around the periphery of a surface cross section is indicated by the length and direction of the arrows. Clearly, the peaks and troughs are not uniformly spaced geometrically around the indented periphery: both the wavelength and amplitude are smaller near the lobes. However, this apparent irregularity is greatly reduced when the fluctuations are analysed in the more appropriate straight-field-line coordinate system referred to above. In Fig. 22, the variation of phase for a typical single-mode oscillation is plotted against the magnetic coordinates $\theta$ and $\phi$, clearly showing a quite regular phase variation in this system. From Fig. 22 we find that the wave propagation in the magnetic field line reference frame is best fitted by mode numbers $m = 3$ and $n = 5$ respectively. We may compare this wave structure with that of the confining magnetic field $B_0$: by calculation the rotational transform $\iota$ in the region of maximum wave field is

$$\iota \sim 1 \cdot 33 \quad (4/3).$$

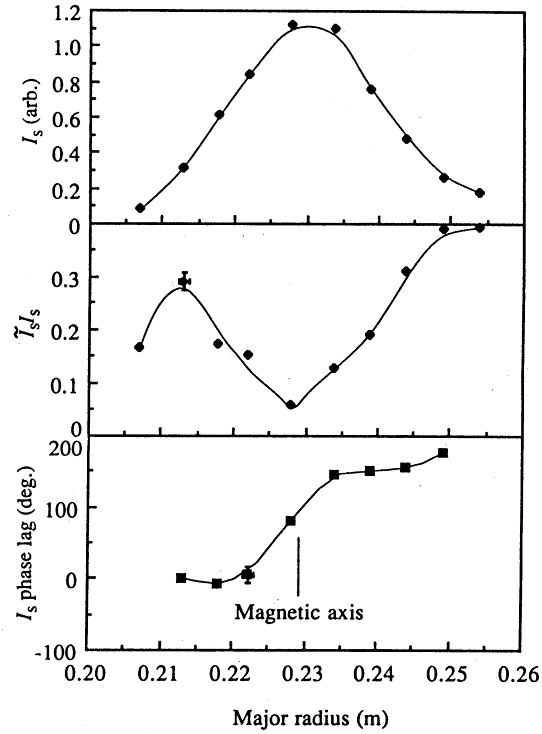


**Fig. 20.** Radial scan of fluctuation amplitude (deduced from the ion saturation current and normalised to the local density) and phase at $\phi = 120°$ for argon, $B_0 = 0 \cdot 125$ T, $n_{e0} = 1 \cdot 8 \times 10^{18}$ m$^{-3}$ and $T_e = 5$ eV).

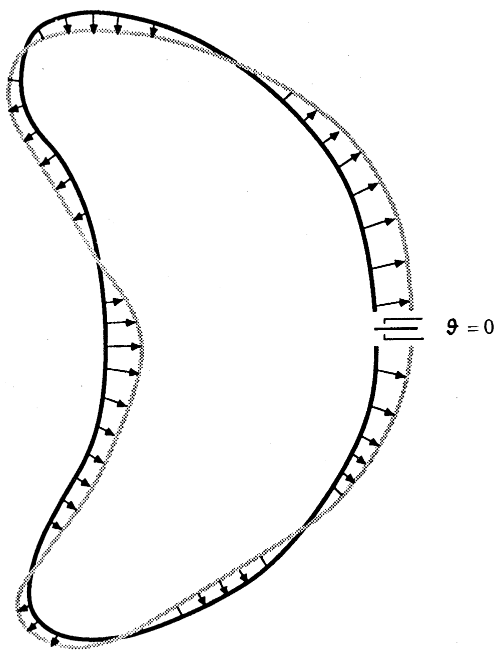


**Fig. 21.** Density fluctuations plotted as displacements at the point of measurement along the magnetic surface $X = 1 \cdot 5$. The real part of the complex amplitude (with reference to the point marked by the probe symbol) is shown.

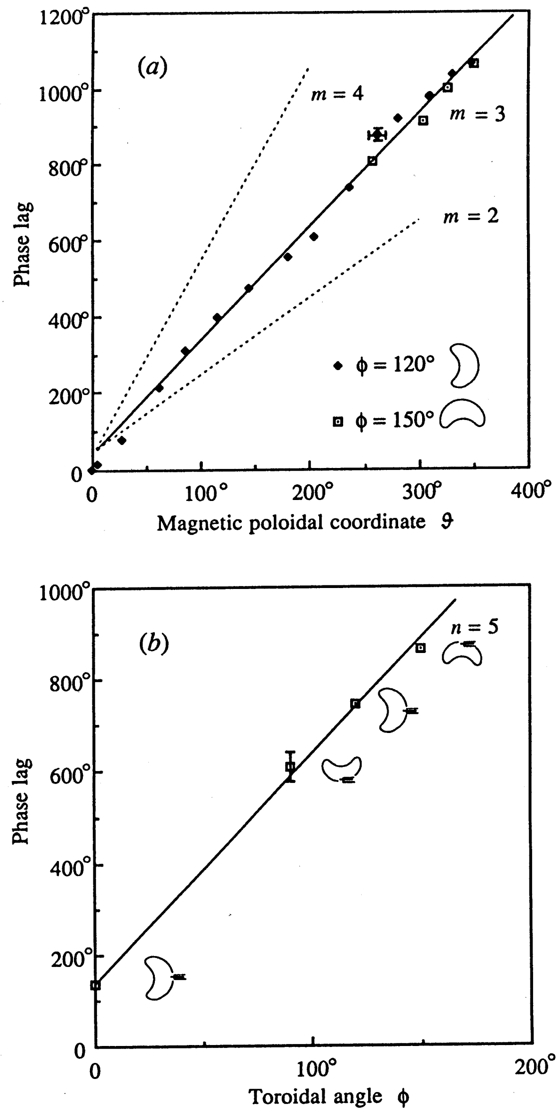


**Fig. 22.** Phase of density fluctuations at $X = 1\cdot 5$ (as for Fig. 20) as a function of (*a*) magnetic poloidal coordinate $\vartheta$ and (*b*) toroidal angle $\phi$. The data are best fitted by $m = 3$ and $n = 5$.

The transform in the *helical* system used above (see the Appendix) is related to $\iota$ by $\iota_h = 3 - \iota \sim 5/3 = n/m$, i.e. the helical structure of the wave matches that of the magnetic field.

By energising the helical winding the rotational transform can be varied, as shown in Fig. 23. When this is done the mode structure of the drift wave is changed. An example of this is the case in which the rotational transform is

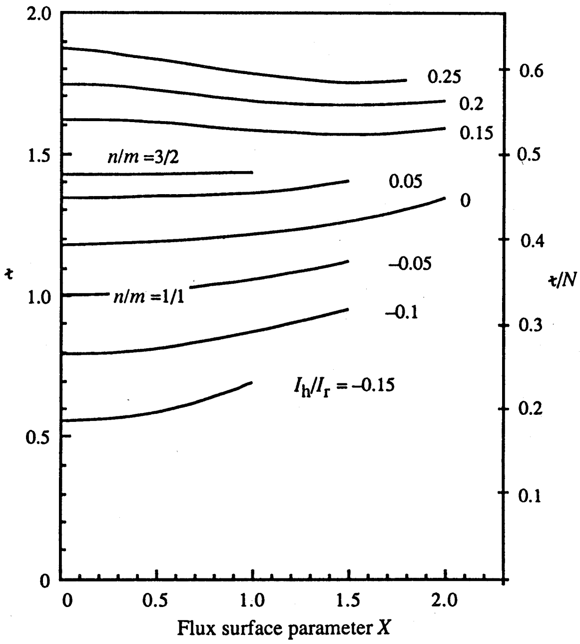


**Fig. 23.** Variation of rotational transform with $X$ and helical core current ratio $I_h/I_r$.

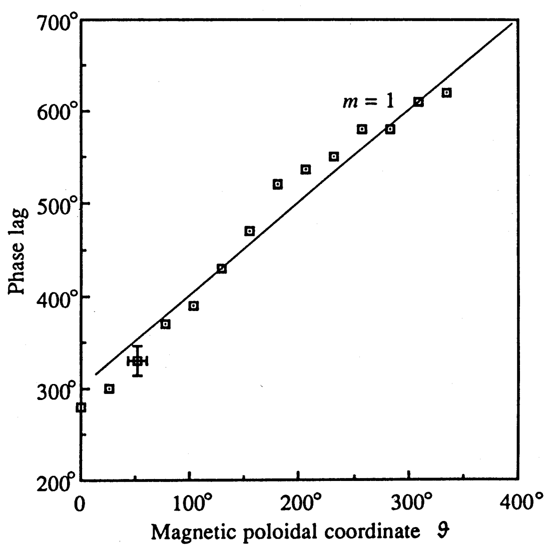


**Fig. 24.** Phase of density fluctuations at $X = 0 \cdot 7$, $\phi = 120°$ for $I_h/I_r = -0 \cdot 05$ as a function of magnetic poloidal coordinate $\theta$. The data are best fitted by $m = 1$ for argon, $B_0 = 0 \cdot 095$ T, $n_{e0} = 9 \times 10^{17}$ m$^{-3}$ and $T_e = 10$ eV).

$\iota \approx 1$, so that $\iota_h \approx 2$. This time the wave pattern is best fitted by mode numbers $m = 1$ and $n = 2$, which again matches the magnetic field helical structure:

$$\iota_h \sim n/m = 2 .$$

Fig. 24 shows the azimuthal variation of phase for this case. Such agreement between the measured wave-field structure and that of the computed magnetic field has been found for a wide range of magnetic configurations, and can be interpreted as an experimental verification of the calculated rotational transform.

A more detailed account of the dispersion, eigenstructure and nature of these fluctuations and of their relation to the plasma confinement, will be presented in a separate paper.

## 6. Discussion

The results outlined above for the plasma equilibrium distributions are all consistent with the existence of closed, nested, helical flux surfaces, whose various geometries in all cases agree within measurement accuracy with those calculated from the currents which actually flow in the conductors. Those low-order helical eigenmodes of self-excited plasma oscillations which can be studied in sufficient detail are also consistent with the calculated trajectories of the field lines themselves in the outer region of the plasma. A more precise measurement of the rotational transforms on individual surfaces (which relies on the near coincidence between the guiding-centre orbits of a low-energy electron beam and the field-line trajectories) remains to be performed.

The small size of the apparatus precludes any but the most qualitative observations of its global energy confinement properties. For example, under the conditions prevailing in the experiments just described, much of the electrical power supplied to the plasma is dissipated via inelastic collisional processes. Thus, any comparison of these energy confinement times with those of other magnetic confinement devices containing essentially fully ionised plasma would require subtraction of this rather large fraction from the input power to SHEILA. This result would be too inaccurate to be worth while. However, we can make a crude estimate of the global lower limit confinement based on the measured total thermal energy content of the plasma and the r.m.s. power supplied to the ohmic heating primary winding (the poloidal ring) by ignoring both inelastic and copper losses. For example, take a typical discharge in which the RF amplifier supplies about 300 W to maintain a mean plasma density $n_e \approx 2 \times 10^{18}\ \mathrm{m}^{-3}$ at a mean temperature $T_e \approx 6$ eV. Since the plasma volume is $V = 4 \times 10^{-3}\ \mathrm{m}^3$, the global energy replacement time is

$$\tau_E = \frac{3}{2}\,\frac{n_e T_e V}{P} \sim 4 \times 10^{-5}\ \mathrm{s}.$$

For comparison, we can estimate the confinement time to be expected for a tokamak of comparable size and density, using the best available empirical scaling laws, to be of order $3\times10^{-6}$ s, much less than observed in the heliac even when no account is taken of inelastic losses.

The results obtained in this small apparatus are adequate to confirm the existence of the surfaces and their geometry. However, to extend these studies to such important topics as the effect of magnetic geometry in transport of particles and heat, the effect of shear and magnetic wells on stability, the effect of finite plasma pressure on both equilibria and stability, etc., requires a significant increase in both size and operating field strength in order to achieve the required plasma conditions. The main parameters of such an apparatus, known as H-1, which is currently under construction are compared with those of SHEILA in Table 1.

## Acknowledgments

The authors gratefully acknowledge discussions with T. K. Chu, R. L. Dewar, A. Butcher-Ehrhardt, H. J. Gardner, W. N.-C. Sy and C. F. Vance; R. Gresham for mechanical design; J. T. Elso for the initial field calculations; A. D. Campbell, G. J. C. Davis, E. A. Fox, R. Goldberg, R. J. Kimlin, G. McCluskey, N. Trama, J. Wach, E. Wedhorn and D.-F. Zhou for technical contributions; and the R.S.Phys.S. mechanical workshop for construction. We especially acknowledge the contribution of the late J. W. Blamey for his enthusiastic engineering support of the heliac project. This was the last of his many contributions to the work of the Research School.

## References

Allis, W. P., and Brown, S. C. (1952). *Phys. Rev.* **87**, 419.
Bauer, F., Betancourt, O., and Garabedian, P. (1984). 'Magnetohydrodynamic Equilibrium and Stability of Stellarators' (Springer: New York).
Blackwell, B. D. (1988). The Bline Field Line Code. Aust. Nat. Univ. Int. Rep. ANU-PRL TR88/6.
Blackwell, B. D., Dewar, R. L., Gardner, H. J., Hamberger, S. M., Sharp, L. E., Shi, X.-H., Vance, C. F., and Zhou, D. F. (1987). Proc. 11th Int. Conf. on Plasma Physics and Controlled Fusion Research, Kyoto 1986, Vol. 2, p. 511 (IAEA: Vienna).
Blackwell, B. D., Hamberger, S. M., Sharp, L. E., and Shi, X.-H. (1985). *Nucl. Fusion* **25**, 1485.
Blackwell, B. D., and Shi, X.-H. (1988). Breakdown and Plasma Formation in the SHEILA Heliac. Aust. Nat. Univ. Int. Rep. ANU-PRL TR88/4.
Bolton, R. A. E., Hoffmann, C. R. J., Lees, D. J., Medley, S. S., Millar, W., Reynolds, P., *et al.* (1971). *Phys. Fluids* **14**, 1566.
Boozer, A. H. (1981). *Phys. Fluids* **24**, 1999.
Boozer, A. H., Chu, T.-K., Dewar, R. L., Furth, H. P., *et al.* (1983). Proc. 9th Int. Conf. on Plasma Physics and Controlled Fusion Research, Baltimore 1982, Vol. 3, p. 129 (IAEA: Vienna).
Brown, S. C. (1959). 'Basic Data of Plasma Physics' (MIT Press: Cambridge, Mass.).
Carreras, B. A., Grieger, G., Harris, J. H., Johnson, J. L., *et al.* (1988). *Nucl. Fusion* **28**, 1613.
Conway, G. D. (1988). ECRH Experiments with a 2·45 GHz Magnetron. Aust. Nat. Univ. Int. Rep. ANU-PRL TR88/2.
Courbold, M. A., and How, J. A. (1984). *Comput. Phys. Commun.* **32**, 231.
Dewar, R. L., Monticello, D. A., and Sy, W.-N. (1984). *Phys. Fluids* **27**, 1723.
Ehrhardt, A. B. (1984). Fifth Int. Workshop on Stellarators, Proc. IAEA Tech. Comm. on Plasma Confinement and Heating in Stellarators, Schloss Ringberg, Sept. 1984, Vol. 2 (Eds F. Rau and G. G. Leotta), p. 717 (IAEA: Vienna).
Ehrhardt, A. B. (1985). Heliac User's Guide, Jan. 1985. Princeton Plasma Physics Lab. Int. Rep.
Furth, H. P., Killeen, J., Rosenbluth, M. N., and Coppi, B. (1966). Proc. 2nd Int. Conf. on Plasma Physics and Controlled Fusion Research, Culham 1965, Vol. 1, p. 103 (IAEA: Vienna).

Furth, H. P., and Rosenbluth, M. N. (1964). *Phys. Fluids* **7**, 764.
Gibson, A. (1967). *Phys. Fluids* **10**, 1553.
Hamada, S. (1962). *Nucl. Fusion* **2**, 23.
Hamberger, S. M., Sharp, L. E., and Malein, A. (1975). Proc. 5th Int. Conf. on Plasma Physics and Controlled Fusion Research, Tokyo 1974, Vol. 2, p. 21 (IAEA: Vienna).
Harris, J. H., Cantrell, J. L., Hender, T. C., Carreras, B. A., and Morris, R. N. (1985). *Nucl. Fusion* **25**, 623.
Hirshman, S. P., and van Rij, W. I. (1986). *Comput. Phys. Comm.* **43**, 155.
MacDonald, A. D. (1966). 'Microwave Breakdown in Gases' (Wiley: New York).
McNamara, B., Whiteman, K. J., and Taylor, J. B. (1966). Proc. 2nd Int. Conf. on Plasma Physics and Controlled Fusion Research, Culham 1965, Vol. 1, p. 145 (IAEA: Vienna).
Reiman, A. H., and Boozer, A. H. (1984). *Phys. Fluids* **27**, 2446.
Shi, X.-H., Hamberger, S. M., and Blackwell, B. D. (1988). *Nucl. Fusion* **28**, 859.
Shyn, T. W., and Sharp, W. E. (1981). *Phys. Rev.* A **24**, 1734.
Spitzer, L., Jr (1958). *Phys. Fluids* **1**, 253.
Swift, J. D., and Schwar, M. J. R. (1970). 'Electrical Probes for Plasma Diagnostics', p. 144 (Iliffe: London).
Yoshikawa, S. (1983). *Nucl. Fusion* **23**, 667.

## Appendix: Magnetic Surfaces

In rotating helically about the minor and major axes of a torus [i.e. in both poloidal angle $\theta$ and toroidal angle $\phi$ respectively, where $(r, \theta, \phi)$ are quasi-toroidal coordinates], appropriate magnetic field lines can trace out *magnetic surfaces*. Surfaces are considered to be closed when the field line, if followed sufficiently far, either closes on itself or covers a surface which encloses some toroidal volume $V$ and contains a definite magnetic flux known as the toroidal flux $\psi$. (In the absence of symmetry about the major axis no rigorous proof is available that any closed toroidal surfaces exist.) In general, such toroidal surfaces form a nested set, of which the one with vanishingly small cross section ($\psi = 0$) forms the *magnetic axis*. The change in poloidal angle $\theta$ subtended by a field line with respect to the minor geometric axis for one toroidal rotation is called the *rotational transform* $\iota$. (The definition is strictly true only in straight field line coordinates—quasi-toroidal coordinates may be used if $\iota$ is averaged over a field line.) The transform $\iota$ is usually expressed in units of $2\pi$: $\iota\!\!\text{-} = \iota/2\pi$, and is a constant of each surface.

The reciprocal of $\iota\!\!\text{-}$ is the 'safety factor' $q$ used in tokamak theory. Surfaces for which $\iota\!\!\text{-}_h = n/m$, where $n$ and $m$ are integers, are termed *rational*. If $n, m$ correspond to toroidal, poloidal mode numbers of some field perturbation, the surface is *mode rational*. In general such resonant interaction leads to the formation of *magnetic islands* centred around the appropriate rational surface, whose widths depend on the magnitude of the perturbation. The variation of $\iota\!\!\text{-}$ with surface $X$ is known as *shear*, conventionally called positive if $\{\iota\!\!\text{-}(X) - \iota\!\!\text{-}(0)\}/\iota\!\!\text{-}(0) > 0$ where $X = 0$ is the magnetic axis. The shear limits the extent of the resonance, and thus the island width.

A *magnetic well* is said to exist in a magnetoplasma if the field strength $|\boldsymbol{B}|$ increases outwards in all directions from its centre. Since in a torus this can occur only in an average sense, $|\boldsymbol{B}|^{-1}$ is replaced by

$$V' = \frac{dV}{d\psi} = \lim_{\phi \to \infty} \frac{2\pi}{\phi} \int \frac{dl}{B},$$

where $V(\psi)$ is the volume of the flux surface containing toroidal flux $\psi$, and $l$ is the length of a field line on the surface. The quantity $\{V'(0)-V'(\psi)\}/V'(0)$ is the depth of the mean magnetic well. In general, both shear and magnetic wells are stabilising features.

For some purposes it is more convenient to use a coordinate system in which the field lines are straight (Hamada 1962; Boozer 1981; Dewar *et al.* 1984), with a flux surface coordinate, e.g. $\psi$, replacing the radial coordinate. In this paper we have used a variant of the PEST coordinate system $(\psi, \vartheta, \phi)$(Dewar *et al.* 1984) in which the toroidal angle is identical with the quasi-toroidal angle $\phi$. Very similar results are obtained for the data of Figs 22 and 23 if Boozer's system is used.

In magnetic coordinates the natural rotational transform in a frame which rotates about the magnetic axis in synchronism with the 'bean' shape of the heliac $\iota_h$ is related to that in the toroidal (or laboratory) frame $\iota$ by

$$\iota_h = N - \iota,$$

where $N$ is the number of helical rotations made by the axis ($N=3$ in SHEILA).

It is not always convenient to use this coordinate system for experimental work, because the flux surface label $\psi$ depends on the current in the magnetic field coil set if an absolute measure of $\psi$ is used, or the choice of the outermost surface if $\psi$ is measured relative to the flux contained within that surface. (In 2D, the last surface is a separatrix and thus clearly defined, but in 3D, the outer surface quality degrades continuously as more magnetic island chains appear, the magnetic field ripple increases, and the magnetic well disappears.) We have therefore introduced an alternative flux label $X$ which we use, instead of the usual label $\psi$, in this paper in situations where precise specification of a particular surface is required.

In the absence of plasma the magnetic surfaces can be calculated with arbitrary precision by following magnetic field lines due to external conductor currents. The presence of plasma with finite pressure introduces a distributed current into the equilibrium required to satisfy pressure balance:

$$\boldsymbol{J} \times \boldsymbol{B} = \nabla p .$$

This self-consistent current density $\boldsymbol{J}$ modifies the magnetic surfaces, in general changing both their shape and position (not significantly for SHEILA in this paper). Appropriate harmonics of $\boldsymbol{J}$ may resonate, both linearly and non-linearly, with rational surfaces, and can affect both the equilibrium and its stability (Reiman and Boozer 1984). The absence of symmetry makes analytic solution impossible and the problem requires fully three-dimensional numerical calculation for which large computer codes such as BETA (Bauer *et al.* 1984) and VMEC (Hirshman and van Rij 1986) have been developed.

Manuscript received 3 October, accepted 15 November 1988